Chiral Discrimination by Vibrational Spectroscopy Utilizing Local Modes

ELFI KRAKA,* MAREK FREINDORF, AND DIETER CREMER

Computational and Theoretical Chemistry Group, Department of Chemistry, Southern Methodist University, 3215 Daniel Ave., Dallas, TX 75275-03114

ABSTRACT Chiral discrimination of homochiral and heterochiral H-bonded complexes is a challenge for both experimentalists and computational chemists. It is demonstrated that a two-pronged approach based on far-infrared vibrational spectroscopy and the calculation of local mode frequencies facilitates the chiral discrimination of H-bonded dimers. The local H-bond stretching frequencies identify the strongest H-bonds and by this the dominating chiral diastereomer. This is shown in the case of peroxide, trioxide, hydrazine, glycidol, and butan-2-ol dimers as well as propylene oxide···glycidol complexes investigated with the help of second-order Møller–Plesset perturbation, coupled cluster, and density functional theory calculations where, in the latter case, the ωB97X-D functional was used for an improved description of H-bonding. In some cases, additional intermolecular interactions overrule the important role of H-bonding, which is found by calculating chirodiastaltic energies. *Chirality 25:185–196, 2013.* © 2013 Wiley Periodicals, Inc.

KEY WORDS: chiral discrimination; chiral recognition; local vibrational modes; H-bonding; chirodiastaltic energy; decomposition of normal modes

INTRODUCTION

Chirality is a fundamental chemical property, which has drawn the attention of chemists and physicists since its discovery in the 19th century.[1–3] Most biochemical processes in living organisms involve chiral interactions.[4] A fascinating fact, still not well understood today, is the homochirality of life. Biomolecules tend to be homochiral, i.e., they are made up from units of the same chirality.[5] The amino acid building blocks of proteins in human beings all possess the L configuration whereas their D enantiomers are the building blocks for bacteria cell walls. Nucleic acids are built from D- rather than L-configured sugars.[6]

The ability of a chiral probe to differentiate between the two enantiomers of a chiral molecule (chiral recognition) is of relevance in biochemistry,[7] analytical chemistry,[8,9] asymmetric organic synthesis,[10] catalysis,[11] polymer and material design, and in drug design.[12,13] Chiral recognition is based on a sensitive interplay of inter- and intra-molecular non-covalent interactions,[14] which come into play when the reacting partners approach each other. For example, hydrogen bonding plays a key role[15] with regard to supramolecular chirality[16] or in molecular imprinting.[17] Another important factor in chiral recognition is the conformational flexibility of a chiral diastereomer.[18] Different conformers of a molecule may show different recognition profiles toward a given target, e.g., different types and numbers of hydrogen bonds or other stabilizing non-covalent interactions may be established.

In order to understand the mechanism of chiral recognition much effort has been invested in recent years into the study of chiral discrimination, utilizing either experimental[19,20] or theoretical means.[21] Studies at the molecular level are still a challenge because energy differences between diastereomeric pairs distinguished only by their homo- and heterochirality are small, as are the differences in other molecular properties.[22,23]

One popular way of distinguishing between homochiral and heterochiral dimers is the chirodiastaltic energy ΔE_{chir}, introduced by Portmann and coworkers.[24] It is defined as the energy difference between homochiral and heterochiral complexes, generally expressed as the difference in complex binding energies of homo- and heterochiral complexes. Experimentally, these binding energies can be derived, for example, from resonance-enhanced two- or multi-photon ionization[25] spectra if an aromatic chromophore is present in the target system. Such energy differences may be in the 0.5 kcal/mol range, which makes measurements challenging.[26] The calculation of complex binding energies is also challenging because relatively small errors in the calculations can falsify the results. Apart from this, one has to consider that complex binding energies, similar to bond dissociation energies, contain the reorganization and relaxation effects of the monomers when generated in the decomposition of the complex, and in this way the binding energies are artificially decreased. Only the intrinsic complex binding energy (dissociation of the complex into monomers frozen in the geometry and electron density distribution they have in the complex) would lead to an appropriate energy-based descriptor for the strength of binding in the complex.[27] Such a binding energy is a cumulative property and does not allow detailed insight into the electronic factors stabilizing the dimer. Therefore one has to be cautious about directly relating the chirodiastaltic energy ΔE_{chir} to the difference in H-bond energies[28].

Optical and vibrational circular dichroism (OCD and VCD) spectroscopy have been successfully applied in the investigation of chiral molecules. Also, the calculation of chiroptical properties has become a powerful tool.[29,30] Although OCD and VCD spectroscopy have been mostly applied to distinguish enantiomers, in selected cases these methods have also proven to be useful for the determination of the absolute configuration of diastereomeric structures. A recent example is the chiral recognition of of diastereomeric 6-cedrols by

Contract grant sponsor: National Science Foundation; Contract grant number: 1152357.
*Correspondence to: Elfi Kraka, Computational and Theoretical Chemistry Group, Department of Chemistry, Southern Methodist University, 3215 Daniel Ave., Dallas, TX 75275–03114, USA. E-mail: ekraka@smu.edu
Received for publication 25 July 2012; Accepted 12 October 2012
DOI: 10.1002/chir.22130
Published online 18 January 2013 in Wiley Online Library (wileyonlinelibrary.com).

© 2013 Wiley Periodicals, Inc

VCD.[31] Recently, Del Bene and coworkers[32] investigated whether NMR spin-spin coupling constants (SSCCs) may be a tool for chiral discrimination. They found that, in most cases, the values of the spin-spin coupling constants differ only marginally so that they cannot be used for chiral discrimination. Fourier transform microwave spectroscopy has been applied to distinguish small structural differences between diastereomers provided they have a sufficiently large dipole moment. For example, King measured the first complete rotational spectrum of the most stable heterochiral 2-butanol dimer.[33]

Vibrational spectroscopy has been frequently employed for chiral discrimination in the form of jet expansion Fourier-transform infrared (FTIR) spectroscopy, in connection with laser-induced fluorescence, or in the form of double resonance experiments of the IR-UV type.[15,34,35] Most of these efforts focused on the O-H and N-H stretching modes, attempting to characterize the dimers via red/blue shifts of the corresponding frequencies upon dimerization. Feng and coworkers[36] as well as Zielke and Suhm[37] suggested a direct characterization of H-bond stretching modes in the far infrared (FIR) frequency range. Although one can identify a mode and its associated frequency, which is dominated by H-bond stretching character,[15,23,38] the exact character of this particular mode as it results from mode-mode coupling cannot be determined experimentally. This can only be done by a local mode decomposition analysis[39] which has been applied by Freindorf, Kraka, and Cremer (hereinafter, FKC)[28] for a comprehensive analysis of H-bonding using the local vibrational modes first introduced by Konkoli and Cremer.[40,41]

We will base chiral discrimination on vibrational spectroscopy by determining the local H-bond stretching modes of homo- and heterochiral pairs of complexes, which have been the target of recent investigations. As shown by FKC, the strength of H-bonding, and thereby to some extent also the stability of a H-bonded complex, can be assessed by the frequency and force constant of the local H-bond stretching mode.[28] Local mode force constants lead to bond orders characterizing H-bonding from relatively strong to weak interactions. FKC showed that there is no correlation between local mode force constants and complex binding energies, in line with the above discussion. Xue and Suhm came to a similar conclusion:[42] Their H-bonding force constants for carboxylic acid dimers, derived via a pseudodiatomic model, do not correlate with the complex binding energies.

In the section immediately following, we will present our strategy for chiral discrimination based in local vibrational modes and briefly summarize the theory of local vibrational modes. The computational methods employed in this work are then described in Computational Details. The investigation of 26 homo- or heterochiral H-bonded complexes is presented in Results and Discussion. The last section summarizes our conclusions and provides an outlook on how FIR vibrational spectroscopy can be used as a powerful tool for chiral discrimination.

Chiral Discrimination Based on Local Vibrational Modes

The strategy for chiral discrimination based on vibrational spectroscopy, as used in these computational and future experimental investigations, is outlined in Scheme 1. Starting from either experimental or calculated normal mode frequencies (step I in Scheme 1) the theory of local vibrational modes, originally developed by Konkoli and Cremer,[40,41] is applied to derive local vibrational stretching frequencies associated with the non-covalent intermolecular interactions from normal mode frequencies of the chiral complexes in question (step II in Scheme 1). In this work (for the complexes investigated, see Scheme 2), these are different types of H-bonds; however, in general, this can be any type of non-covalent interaction leading to some degree of bonding. Chiral

Chiral Discrimination based on Vibrational Spectroscopy

I Collection of data	Determination of normal mode frequencies *(Experiment or computations)*
II Preparation of data	Transformation into local mode frequencies *(Computations)*
III Chiral discrimination	Identification of decisive intermolecular interactions utilizing local mode frequencies Rationalization of chirodiastaltic energies *(Analysis)*
IV Computational verification	Determination of additional factors influencing chirodiastaltic energies: electronic factors, solvation, entropic factors, etc *(Computations)*
V Experimental verification	Identification of normal mode frequencies, which lead to chiral discrimination via the measured vibrational spectra *(Experiment)*

Scheme 1. Five steps of chiral discrimination based on vibrational spectroscopy.

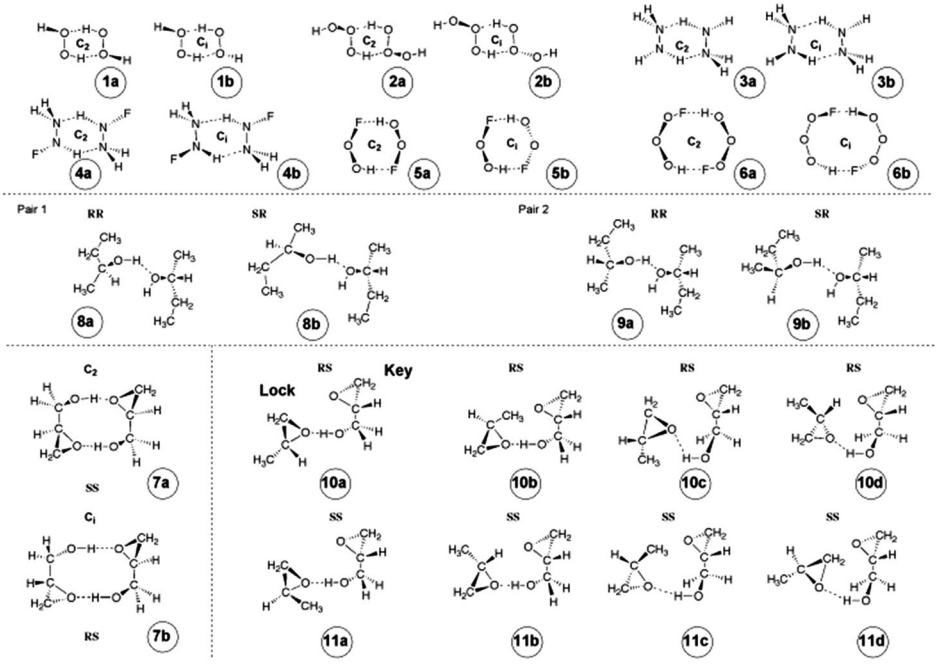

Scheme 2. Molecules investigated in this work.

discrimination (step III, Scheme 1) will be based on the H-bond strengths as determined by the local H-bond stretching frequencies. Each prediction will be qualitatively tested by comparing relative stabilities based on the H-bond strength with the calculated chirodiastaltic energies. In the case of contradictory outcomes, additional stabilizing factors resulting from electronic, solvation, entropic, or other effects will be evaluated utilizing computational means (step IV, Scheme 1). In this way, intermolecular interactions can be identified, which may outweigh energy differences resulting from H-bonding. Finally (step V, Scheme 1), normal modes with dominating H-bond stretching character determined experimentally will be related via an adiabatic connection scheme to the local H-bond stretching modes[39] and their composition will be determined via the local mode analysis of Konkoli and Cremer.[41] This leads to a two-pronged approach, in which each quantum chemical prediction can be verified by suitable measurements of the complex vibrations. It is noteworthy in this connection that minor differences in the normal mode frequencies may be related to relatively large differences in the corresponding local mode differences (as a result of mode-mode coupling and other effects) where only the knowledge of the latter guarantees the correct interpretation of the former frequencies. Clearly, chiral discrimination as described in Scheme 1 involves the interplay of measurements and computations. In this work, however, we will outline the usefulness of the strategy given in Scheme 1 by exclusively using the results of quantum chemical investigations.

Determination of Local Vibrational Modes

Konkoli and Cremer[40] solved the problem of obtaining local vibrational modes in two different ways leading to the same results. They first solved the Euler–Lagrange equations of vibrational spectroscopy for an n-atomic molecular fragment described by Cartesian coordinates. They showed that by suppressing mass coupling (via the kinetic energy term) local vibrational modes were obtained.[40] Then they derived the formalism for internal coordinates by assigning an internal displacement coordinate for the same n-atomic molecular fragment that leads its local mode (*leading parameter* principle).[40] When solving the Euler–Lagrange equations under the constraint that the geometry of the remaining molecule is relaxed upon a fixed displacement of the leading parameter, the same local vibrational modes were obtained as in the first approach. Based on the second approach, the local vibrational modes obtained were dubbed adiabatic internal coordinate modes.[40]

The determination of local modes requires solving the Wilson equation of vibrational spectroscopy[43]

$$\mathbf{F}^{q}\mathbf{D} = \mathbf{G}^{-1}\mathbf{D}\mathbf{L} \tag{1}$$

where $\mathbf{F}^{q}$ is the force constant matrix expressed in internal coordinates, matrix $\mathbf{G}$ is the Wilson G matrix, matrix $\mathbf{D}$ contains the normal mode vectors $\mathbf{d}_{\mu}$ ($\mu = 1, \ldots 3N\text{-}L$; N: number of atoms; L: number of translations and rotations) as column vectors, and the diagonal matrix contains the eigenvectors $4\pi^2c^2\omega_{\mu}{}^2$ (c, speed of light; ω_{μ}, normal mode frequency). By expressing the force constants in normal coordinates Q_{μ}, the diagonal matrix $\mathbf{K}$ is obtained, which is needed for determining local mode vectors $\mathbf{a}_n$ associated with internal coordinate displacements q_n:[40]

$$\mathbf{a}_n = \frac{\mathbf{K}^{-1}\mathbf{d}_n^{\dagger}}{\mathbf{d}_n\mathbf{K}^{-1}\mathbf{d}_n^{\dagger}} \tag{2}$$

where $\mathbf{d}_n$, contrary to $\mathbf{d}_{\mu}$, is a row vector of matrix $\mathbf{D}$. The local modes are characterized by force constants k_a^n (subscript a for adiabatic)

$$k_a^n = \mathbf{a}_n^{\dagger}\ \mathbf{K}\ \mathbf{a}_n \tag{3}$$

and vibrational frequencies ω_a^n

$$4\pi^2 c^2 \left(\omega_a^n\right)^2 = k_a^n \, G_{nn} \quad (4)$$

where G_{nn} is a diagonal element of matrix **G** and corresponds to the reduced mass of local mode $\mathbf{a}_n$.[40] Each local mode has an infrared intensity, which relates to the effective partial charges of the atoms of a fragment.[44] The local modes of Konkoli and Cremer lead to vibrational frequencies that are identical or close to frequencies measured for normal modes with dominating local character.[45–48] The delocalized character of normal modes is preferentially caused by mass coupling. McKean has shown in about a dozen publications that *isolated CH stretching frequencies* are associated with mass-decoupled modes, which result from a clever isotope substitution pattern and approximate the local modes closely.[46] This was later confirmed by Larsson and Cremer,[47] who compared McKean's isolated CH stretching frequencies with the local mode frequencies. A similar observation could be made for the frequencies extracted from overtone spectroscopy.[48] Local and normal vibrational modes are uniquely related where this relationship can be illustrated by an adiabatic connection scheme that quantifies the degree of coupling between the local modes.[39,41] In the following, we will use the local modes of Konkoli and Cremer to describe H-bonding. Because only H-bonds are analyzed, we simplify the notation for local mode force constant and frequency to k_a and ω_a, respectively, by deleting the superscript n.

COMPUTATIONAL DETAILS

In this work, the geometry of the 26 diastereomers shown in Scheme 2 (dimers **1–11** with homo- and heterochiral forms) were optimized using two levels of theory and two different basis sets. The characteristics of the H-bond of dimers **1–11** are summarized in Table 1. DFT calculations were carried out with ωB97X-D, which is a long-range corrected hybrid exchange-correlation functional with

TABLE 1. Characterization of H-bonds in complexes (1–11); H-bond length *R*, local mode force constant k_a, local vibrational mode ω_a, normal vibrational mode(s) ω_μ dominated by ω_a as calculated at the ωB97X-D/aug-cc-pVTZ level of theory (1–6), ωB97X-D/aug-cc-pVDZ level of theory (7, 10–11) and MP2/aug-cc-pVDZ (8–9)

Mol	Char	Bond	*R* (Å)	k_a (mdyn/Å)	ω_a (cm^{-1})	$\omega_{\mu 1}$[a] (cm^{-1})	$\omega_{\mu 2}$[a] (cm^{-1})
1a	homo	O···H	1.921	0.164	542	194(47%)	220(31%)
1b	hetero	O···H	1.924	0.167	547	196(49%)	221(31%)
2a	homo	O···H	2.016	0.094	409	152(45%)	166(26%)
2c	hetero	O···H	2.048	0.089	399	149(44%)	168(27%)
3a	homo	N···H	2.234	0.097	419	154(44%)	164(33%)
3b	hetero	N···H	2.212	0.103	432	160(41%)	178(24%)
4a	homo	N···H	2.354	0.069	353	133(25%)	146(21%)
4b	hetero	N···H	2.330	0.047	291	92(34%)	105(18%)
5a	homo	F···H	1.805	0.169	547	198(28%)	217(40%)
5b	hetero	F···H	1.785	0.188	577	214(23%)	230(40)
6a	homo	F···H	1.813	0.164	539	112(29%)	198(37%)
6b	hetero	F···H	2.051	0.006	106	76(6%)	117(24%)
7a	*SS*	H···O	1.837	0.198	596	181(32%)	230(14%)
7b	*RS*	H···O	1.818	0.244	661	147(25%)	201(18%)
8a	*RR*	H···O	1.901	0.164	541	126(30%)	
8b	*SR*	H···O	1.886	0.176	526	124(34%)	
9a	*RR*	H···O	1.881	0.191	584	157(34%)	
9b	*SR*	H···O	1.873	0.189	581	158(26%)	
10a	*RS*	H···O	1.838	0.226	636	210(52%)	
		CH···O	2.555	0.031	237	94(34%)	
		CH···O	2.381	0.060	327	114(60%)	
10b	*RS*	H···O	1.824	0.252	672	203(26%)	
		CH···O	2.483	0.028	225	91(30%)	
		CH···O	2.616	0.008	120	74(14%)	
10c	*RS*	H···O	1.848	0.213	617	193(55%)	
		CH···O	2.483	0.028	225	81(58%)	
		CH···O	2.398	0.031	235	77(47%)	
10d	*RS*	H···O	1.823	0.235	648	192(36%)	
		CH···O	2.518	0.042	273	104(66%)	
		CH···O	2.552	0.048	292	86(63%)	
11a	*SS*	H···O	1.840	0.225	634	196(51%)	
		CH···O	2.510	0.033	244	89(52%)	
		CH···O	2.362	0.059	324	105(64%)	
11b	*SS*	H···O	1.822	0.251	670	216(22%)	
		CH···O	2.593	0.018	178	41(25%)	
		CH···O	2.506	0.032	238	104(65%)	
11c	*SS*	H···O	1.833	0.233	646	188(52%)	
		CH···O	2.558	0.022	201	90(49%)	
		CH···O	2.515	0.038	262	84(42%)	
11d	*SS*	H···O	1.829	0.231	644	225(45%)	
		CH···O	2.560	0.048	294	116(30%)	

[a] Contribution of local mode ω_a is given in parentheses.

empirical dispersion corrections for the description of van der Waals interactions.[49,50] It has been shown that ωB97X-D yields H-bond interaction energies close to results obtained at the CCSD(T) level of theory.[51] We have included some CCSD(T)[52,53] calculations to verify this point (see Table 2). In addition to DFT, second-order Møller–Plesset (MP2) perturbation theory [54,55] was used for two reasons: to compare with DFT results and to compare with MP2 results from the literature (as, e.g., in the case of butan-2-ol dimers **8** and **9**; see Scheme 2).

Calculations for dimers **1–6** and the corresponding monomers were carried out with Dunning's augmented correlation consistent valence triple-zeta basis sets, aug-cc-pVTZ[56,57], whereas complexes **7–11** were investigated employing the corresponding valence double-zeta basis sets, aug-cc-pVDZ.[56,57] Geometry optimizations and vibration frequency calculations at the DFT level were performed with an ultrafine grid applying tight convergence criteria for self-consistent field (SCF) calculations and geometry optimizations. All optimized geometries presented in this article correspond to minima on the potential energy surface as confirmed by the vibrational frequencies, i.e., no imaginary frequencies were found.

Local vibrational modes and their properties (force constants k_a and frequencies ω_a) were calculated from normal vibrational modes according to Konkoli and Cremer,[40] utilizing the program package COLOGNE12.[58] This package was also used for the CNM analysis in terms of local modes.[41] Atomic charges were obtained with the Natural Bond Orbital (NBO) analysis [59–61] as included in the Gaussian program package.[62] The latter program was used for the quantum chemical calculations leading to relative energies ΔE and relative free energies ΔG^0. By assuming an equilibrium between homo- and heterochiral complexes, the equilibrium constant at room temperature was obtained from $\Delta G^0(298)$ differences, which in turn were used to calculate relative concentrations (given in percent) of the chiral complexes assumed to be connected by an equilibrium. For two reasons, $\Delta G^0(298)$ have been complemented by $\Delta G^0(100)$ values. First, spectroscopic measurements of H-bonded complexes are often carried out at reduced temperatures. Second, since harmonic vibrational frequencies were used to calculate enthalpy and entropy corrections, $\Delta G^0(298)$ values may be somewhat exaggerated, which is less problematic when calculating $\Delta G^0(100)$.

Since most of the chiral complexes investigated form rings, the planarity or puckering of these rings was quantitatively determined utilizing the Cremer–Pople puckering coordinates.[63–65] An *N*-membered ring possesses *N*-3 puckering amplitudes and pseudorotation phase angles, i.e., 2 for a five-membered ring, 3 for a six-membered ring, etc. As a result of double H-bonding, the rings formed can adopt only specific nonplanar ring forms, which makes it possible to focus on just one specific puckering amplitude *q* in the discussion. However, for each case considered all *N*-3 puckering coordinates were calculated with the program COLOGNE12.[58]

TABLE 2. Comparison of chirodiastaltic energies (kcal/mol) calculated at the ωB97X-D and the CCSD(T) level of theory[a]

Mol	ωB97X-D	CCSD(T)
1a-1b	0.25	0.37(0.36)[b]
3a-3b	0.56	0.48
4a-4b	0.63	0.34
5a-5b	0.46	0.47(0.47)[b]
6a-6b	−5.84	−5.38
7a-7b	0.59	0.55

[a]CCSD(T) single point calculations at DFT geometries carried out with the same basis set as in the original calculations. [b] Values in parentheses: Geometry optimization at the CCSD(T)/cc-pVTZ level.

RESULTS AND DISCUSSION

The results of this work are presented in Tables 1–3 and Figures 1–5. In the following, we will preferentially discuss calculated local mode frequencies although these frequencies depend (apart from their dependence on the electronic structure) on the mass of the atoms forming a molecular fragment. The local mode force constants are more reliable because they depend only on the electronic effects determining atom-atom interactions. Nevertheless, we stick to the frequencies because they can be much easier related to the measured quantities.

Self-Discrimination in Hydrogen-Bonded Homchiral and Heterochiral Dimers with Axial Chirality

In Figure 1, homo- (*C_2- form, optically active*) and heterochiral dimers (*C_i- form, optically inactive)* of $(HOOH)_2$ (**1**), $(HOOOH)_2$ (**2**), $(H_2NNH_2)_2$ (**3**), $(FHNNH_2)_2$ (**4**), $(FOOH)_2$ (**5**), and $(FOOOH)_2$ (**6**) (see also Scheme 2 and Table 1) are shown. With the exception of the FOOOH dimer ($\Delta E = 5.84$ kcal/mol), chiraldiastaltic energy differences are small (ΔE range: 0.25–0.63 kcal/mol). However, the $\Delta G^0(298)$ values reveal that at room temperature one form dominates between 65% and 99.5%. The dimers form rings that are described in terms of their planarity or puckering with the help of the puckering amplitude *q*.[63]

The equilibrium conformation of hydrogen peroxide possesses a dihedral angle of 110°, which is a result of the avoidance of bond (lone pair) eclipsing and anomeric elocalization of the oxygen pπ electron lone pair into the neighboring σ*(OH) orbital. [66–69] The monomer retains this conformational preference also in the dimer, which has consequences for the intermolecular H-bonds. They involve the pπ(O) lone pair and are best developed when a six-membered ring with two H-bonds is formed. The C_i dimer **1b** adopts an almost planar chair form with one OH bond above and the other below the ring plane (Fig. 1). The slight degree of puckering ($q = 0.076$ Å, Fig. 1) optimizes the orientation of the donor OH bond toward the lone pair of the acceptor and leads to relatively strong H-bonds, as is reflected by a local mode frequency of 547 cm^{-1} similar to that found for the

TABLE 3. Rotational constants (in MHz) of butan-2-ol dimers 8–9

	MP2/aug-cc-pVDZ		
Dimer	A	B	C
8a,*RR*	1854	577	516
8b,*SR*	2170	466	437
9a,*RR*	1792	565	480
9b,*SR*	1558	615	587
		Experimental[a]	
Dimer	A	B	C
9b,*SR*	1569	570	550

[a]Ref. 33.

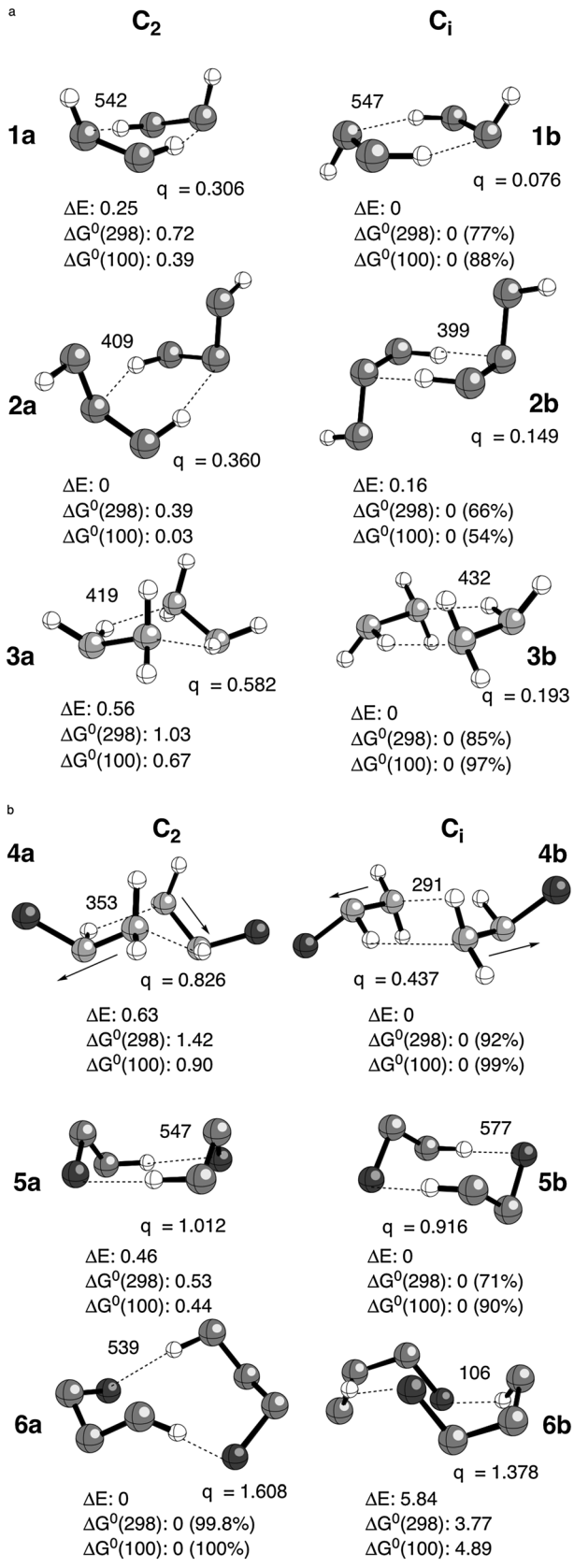

Fig. 1. Hydrogen bond local harmonic vibrational frequencies in cm^{-1}, puckering amplitudes q as well as energy differences ΔE and free energy differences $\Delta G^0(298)$ and $\Delta G^0(100)$ between homo- (C_2)- and heterodimers (C_i) in kcal/mol for molecules **1–6**. ωB97X-D/aug-cc-pVTZ calculations. The relative concentration in % of homo- and heterodimers at room temperature and at 100 K is given in parentheses.

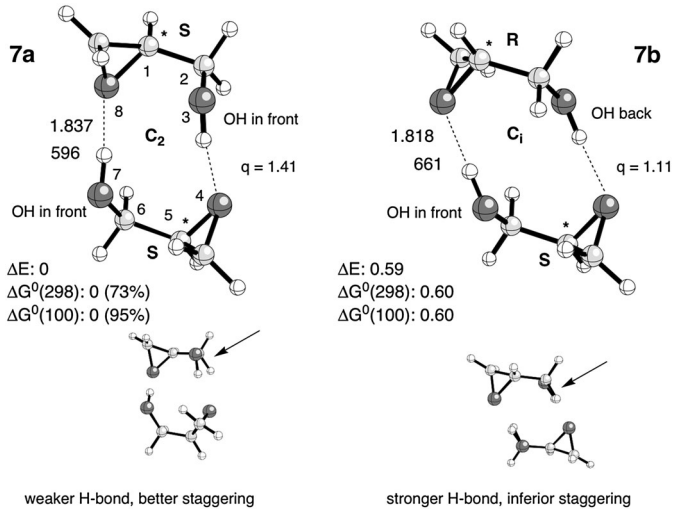

Fig. 2. Hydrogen bond local harmonic vibrational frequencies in cm^{-1}, O···H distances in Å, puckering amplitudes q as well as energy differences ΔE and free energy differences $\Delta G^0(298)$ and $\Delta G^0(100)$ between homo- (C_2)- and heterodimer (C_i) in kcal/mol for glycidol dimer. ωB97X-D/aug-cc-pVDZ calculations. The relative concentration in % of homo- and heterodimer at room temperature and that at 100 K is given in parenthesis.

water dimer.[28] If both external OH bonds are on the same side of the ring as in the C_2-form **1a**, repulsion between the positively charged H atoms (462 melectron, HH distance: 3.81 Å), rotates the monomer units outward and leads to a twist-boat form of the six-membered ring with a significantly larger degree of puckering ($q = 0.306$ Å, Fig. 1). The OH donor bonds are no longer optimally oriented toward the pπ (O) lone pair and accordingly H-bonding is slightly weakened as reflected by a H-bond stretching frequency of 542 cm^{-1}. Repulsion between the (ring-) external H atoms and the weakening of the two H-bonds are responsible for a 0.25 kcal/mol lower stability of **1a**. Also, the six-membered ring of dimer **1a** is more rigid than that of **1b**, which reduces the entropy of **1a** and leads to a larger difference in the free energies between **1a** and **1b** ($\Delta G^0(298) = 0.72$ kcal/mol, Fig. 1).

We note in this connection that the frequencies of local H-bond stretching modes are usually 300–400 cm^{-1} higher than the frequencies of those normal modes being dominated by H-bond stretching. This is a result of mode-mode coupling, mass coupling, and anharmonicity effects, which disguise the actual strength of the H-bond as was shown in the case of water dimer.[70]

The homo- and heterochiral forms of the dihydrogen trioxide dimer **2** also contain a six-membered ring, the stabilities of which are affected by similar electronic interactions as found for **1a** and **1b**. Hence, one would expect **2b** to be more stable than **2a**, which is not the case, because of a third effect not present in **1a** and **1b**. The H-bonds between the monomers are formed involving the pπ lone pair of the central O atom, which is involved in two rather than one anomeric interaction.[71] This makes the pπ electron lone pair less available for H-bonding and the local H-bond stretching frequency is reduced to 399 cm^{-1} (Fig. 1, Table 1). For anomeric delocalization, the monomer should have a HOOO dihedral angle of 90°, which is largely fulfilled for the C_1-symmetrical form **2b** (87°). Repulsion between the external OH groups in **2a** lowers this dihedral angle to 82°, reduces anomeric delocalization of the central pπ electron lone pair, and makes it more available for H-bonding. Consequently, the local H-bond

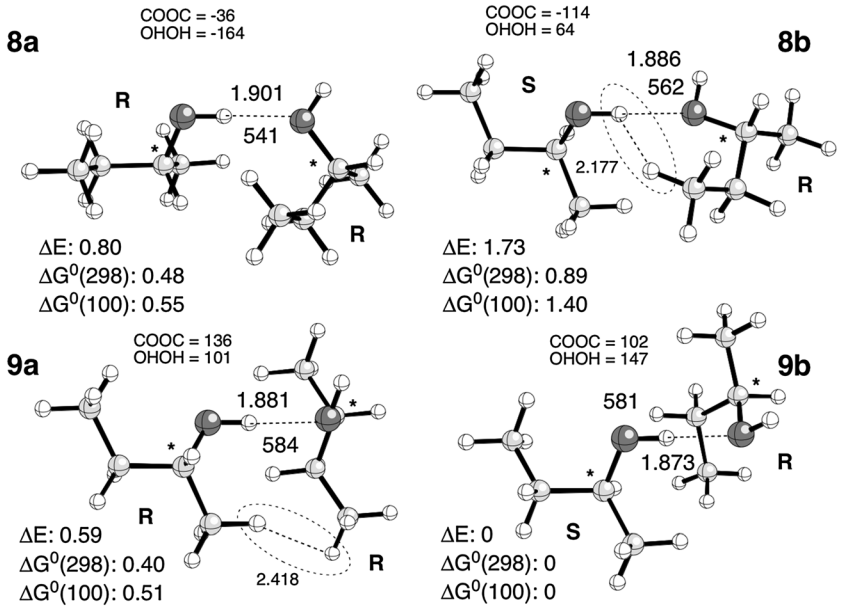

Fig. 3. Hydrogen bond local harmonic vibrational frequencies in cm^{-1}, O···H distances in Å, dihedral angles COOC and OHOH in degree for the two most stable homochiral and two most stable heterochiral butan-2-ol dimers **8–9**. MP2/aug-cc-pVDZ calculations. Energy differences ΔE and free energy differences $\Delta G^0(298)$ and $\Delta G^0(100)$ in kcal/mol are given relative to the most stable form **9b**. Steric repulsion in **8b** and **9a** is encircled.

stretching frequency of **2a** (409 cm^{-1}) is higher than that of **2b** as is its stability (0.16 kcal/mol, Fig. 1). It remains, however, that the six-membered ring of **2a** is more rigid and its entropy lower. Therefore, form **2b** has a 0.39 kcal/mol lower free energy at room temperature than **2a**.

Hydrazine adopts its equilibrium form due to the gauche effect,[69] which also dominates the dimer conformations. Apart from this, the intermolecular interactions of the hydrazine dimers resemble those of the peroxide dimers. The more planar chair form **3b** (Fig. 1) possesses a somewhat stronger H-bond ($\omega_a = 432$ cm^{-1}) than the more puckered C_2-symmetrical form **3a** as reflected by a local mode frequency ω_a of 419 cm^{-1}. Again, the differences are caused by increased steric repulsion between external H atoms in the 1,3 positions of **3a**. It is noteworthy that the entropy and free energy changes between C_i- and C_2-symmetrical forms of **1**, **2**, and **3** are relatively constant, which is a result of the fact that entropic changes are directly related to specific ring forms.

Substitution of one H atom by F in **3** leads to an extra electronic effect, which overwrites differences in H-bonding. This extra-effect results from the large electronegativity of F that (1) leads to a large dipole moment of monofluoro hydrazine (2.32 Debye) and (2) decreases the availability of the electron lone pair at the second N atom for H-bonding as reflected by relatively low H-bond stretching frequencies of 353 and 291 cm^{-1}, respectively (Table 1, Fig. 1). Distortion of the hydrazine geometries leads to more puckered 6-rings (**4a**: $q = 0.826$; **4b** $q = 0.437$ Å). As indicated in Figure 1, form **4b** has the advantage that the molecular dipole moments can align in an antiparallel form almost perfectly, which increases the stability of **4b** via dipole-dipole attraction; however, this also increases the charge transfer from the NH_2 to the NHF group, and by this decreases the availability of the electron lone pair for H-bonding. In **4a**, the molecular dipole moments are aligned at an angle larger than 15°, leading to a reduced attraction and an energy increase ΔE of 0.63 kcal/mol. The weaker H-bonding in the more stable C_i-form **4b** compared to that in the less stable C_2-form **4a** indicates the extra-electronic effect caused by dipole-dipole attraction.

The mono-fluorinated hydrogen peroxide dimer **5**, which forms an eight-membered ring, is more stable, by 0.46 kcal/mol, in the less puckered long-chair form of **5b** than in the long-boat form **5a**. In the long-chair form, the two monomers can get closer together because of smaller electrostatic repulsion. H-bonding is decisive as reflected by the local vibrational H···F stretching frequencies (**5b**: $\omega_a = 577$ cm^{-1}, **5a**: $\omega_a = 547$ cm^{-1}).

For the fluorinated trioxide dimer **6**, the largest differences between the C_i- and C_2-symmetrical form are observed: The local H-bond stretching frequencies differ by 430 cm^{-1} (**6a**: $\omega_a = 539$ cm^{-1}, **6b**: $\omega_a = 106$ cm^{-1}) in line with the large chiral diastaltic energy of 5.8 kcal/mol (Fig. 1). In **6a**, there are two strong anomeric effects per monomer (OOF and OOH), whereas in form **6b** there is just one (OOF). This is a result of the different orientation of the terminal F and H atom in the two chiral forms: In **6a**, the same side orientation (with regard to the OOO-plane of a monomer) makes H-bonding possible without monomer deformation, whereas in **6b** OF and OH group have to rotate by 8° and 37° (relative to the equilibrium conformation in the monomer) to adopt a suitable, but suboptimal position for H-bonding. This explains the large energy difference between **6a** and **6b**. The anomeric effects in **6a** lead to a more negative F and a more positive H atom, thus increasing the electrostatic part of H-bonding.

Obviously, the strength of H-bonding is decisive in five of the six homo/heterochiral pairs investigated. Local vibrational modes disclose which H-bonds are stronger. However, chiral differentiation via H-bond stretching frequencies has to be verified by the chiral diastaltic energies. If this is done, electronic effects, which overrule H-bonding, can be easily identified as in the case of the mono-fluorinated hydrazine dimer **4** for which dipole-dipole attraction becomes decisive. In passing, we note that Del Bene and coworkers[32] recently tried to base chiral discrimination of homo- and heterochiral pairs **1–6** on

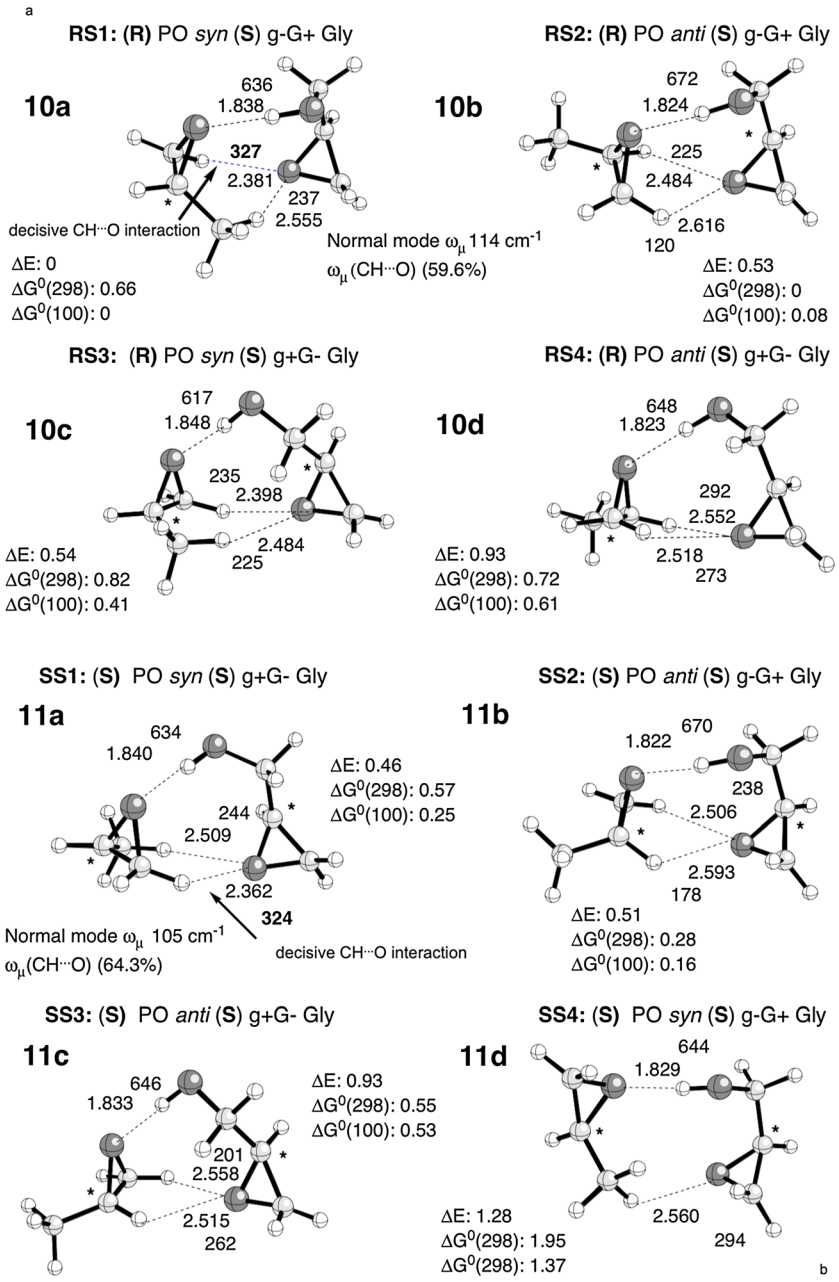

Fig. 4. Hydrogen bond local harmonic vibrational frequencies in cm^{-1}, O···H distances in Å for the PO(O···H) and the two Gly(O···H) bonds for the four most stable (*S*,*R*) heterochiral pairs **10a–10d**, and the four most stable homochiral pairs **11a–11d** of propylene oxide (PO)···glycidole (Gly). ωB97X-D/aug-cc-pVDZ calculations. Energy differences ΔE and free energy differences $\Delta G^0(298)$ and $\Delta G^0(100)$ in kcal/mol are given relative to the most stable form **10a**.

NMR SSCCs. These authors found that the calculated differences in the SSCCs are too small to be detectable experimentally.

Conformationally Rigid and More Flexible Alcohols

Glycidol dimer. Glycidol consists of a rigid oxirane ring with a hydroxy-methylene substituent (Fig. 2, bottom part). Only two conformers were observed so far by jet FTIR spectroscopy with an intensity ratio 4:1.[72] Suhm and coworkers[38,72] carried out supersonic jet FTIR experiments on the chiral discrimination of glycidol dimers. They assigned the main O–H stretching band at 3492 cm^{-1} to homochiral and that at 3488 cm^{-1} to heterochiral dimers.[72] Based on argon expansion studies and confirmed by quantum chemical calculations, they suggested that the most stable complex of two glycidol monomers results from a head-to-tail combination in which the hydroxy-methylene part of each subunit interacts with the oxirane oxygen atom of the other subunit leading to a 10-membered ring that is held together by two H-bonds. The C_2-symmetrical conformer **7a** corresponds to a homochiral (*SS*) form whereas the C_i-symmetrical conformer **7b** is a heterochiral (*RS*) form, both being built from the most stable glycidol conformer (Fig. 2). Caminati and coworkers were able to characterize **7a** via microwave spectroscopy.[73] We will restrict the following discussion to the most stable homo- and heterochiral pair, **7a–7b**.

According to the somewhat larger red shift in the latter case, the heterochiral compound **7b** should have a stronger H-bond and should be more stable. However, the ωB97X-D

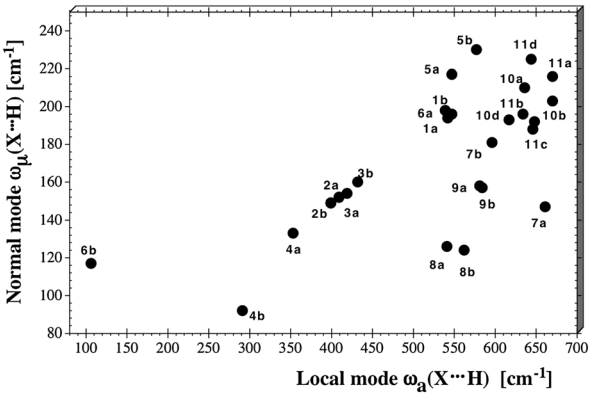

Fig. 5. Correlation between local modes ω_a(X···H) (X = O, N, and F), and normal modes ω_μ(X···H) with largest ω_a(X···H) contribution (see Table 1), for all 26 molecules. All frequencies are given in cm^{-1}. ωB97X-D/aug-cc-pVTZ calculations for molecules **1–6**; MP2/aug-cc-pVDZ calculations for molecules **8** and **9**; ωB97X-D/aug-cc-pVDZ calculations for molecules **7**, **10**, and **11**. In the case of multiple hydrogen bonds, the strongest is given.

calculations reveal that the homochiral dimer **7a** is more stable than the heterochiral dimer **7b**, by 0.59 kcal/mol. Dimer **7b** is less puckered (q = 1.11 Å) compared to **7a** (q = 1.41 Å) and the four oxygen atoms are lying in one plane, whereas in **7a** the OO···OO dihedral angle is 41°. In the planar oxygen arrangement, the two monomers can come closer together as is reflected by a H···O distance of 1.818 Å compared to 1.837 Å found for **7a**. This leads to a stronger H-bond and a larger local H-bond stretching frequency of 661 cm^{-1} compared to 596 cm^{-1} in the case of **7a**, which is in line with the observed red shifts.[38,72] Obviously, H-bonding is not decisive in this case. Other electronic effects play a role. In view of the different orientation of the CH_2OH groups at the stereogenic center (down for *R*; up for *S* with regard to the viewing plane in Fig. 2), the dimers have to adopt different forms: a more rectangular one is possible for the *SS*-form **7a** and a more parallelogram-like *RS*-form **7b**. Accordingly, the CH_2OH groups have to be rotated differently in the dimer to establish effective H-bonds. In **7a** and **7b**, the HCOH dihedral angles of the hydroxy-methylene groups are 27° and 7°, respectively, indicating that bond eclipsing is larger in **7b** than in **7a** (see Fig. 2). The same holds for the OCCO angles within the monomer unit (**7a**: 21.1°; **7b**: 12.3°). Considering that a rotation about the CC bond of methanol or ethylene glycol have barriers of 1 and 2 kcal/mol,[74–76] respectively, bond eclipsing causes the energy difference of 0.59 kcal/mol. To summarize, in the glycidol dimer, chiral discrimination is determined by bond eclipsing caused by the different positioning of the four O atoms with regard to each other, which overwrites the H-bonding strength.

Butan-2-ol dimer. Butanol-2-ol is a flexible molecule that can adopt a number of different conformations. Its dimers are connected by a single H-bond, which makes them much more flexible than dimers **1–7** possessing two H-bonds. Only the most stable heterochiral dimer has been fully characterized by rotational spectroscopy.[33] The jet FTIR spectrum of a homo/heterochiral pair of the 2-butanol dimer shows little chirality discrimination in the O–H-stretching region, which makes it difficult to assign the individual frequencies to the correct diastereomer.[77] We will show in the following that the local vibrational H-bond stretching modes are more decisive.

According to DFT and MP2 calculations, the two most stable homo- and heterodimer pairs correspond to complexes **8** and **9** (see Fig. 4), the geometries of which are close to those calculated by King and Howard.[33] We will focus here on the MP2 results to be able to compare with data from their investigation. The most stable form is heterochiral dimer **9b**. The corresponding homochiral form **9a** is less stable, by 0.59 kcal/mol.

As shown in Table 3, the calculated rotational constants for **9b** agree with the experimental data (deviations: $\Delta A = -11$ MHz, $\Delta B = +45$ MHz, $\Delta C = 37$ MHz, Table 2). The small energy differences between the two chiral forms result from steric repulsion. Steric repulsion prevents the two monomers in **9a** from approaching each other as closely as is possible in **9b**, in line with calculated H···O distances of 1.873 Å (**9b**) and 1.881 Å (**9a**). The relative stabilities of **9b** and **9a** reflect the compromise between a reduction of steric repulsion paid for the price of a weaker H-bond. The H-bond stretching frequency in **9b** is 581 cm^{-1}. The OH donor bond forms an angle of 85° with the CO bond of the acceptor O. In **9a** the H-bond stretching frequencyof 584 cm^{-1} is somewhat larger than that found for **9a**, however the steric repulsion is increased. The OH donor bond in 9a forms an angle of 104° with the CO bond of the acceptor O.

According to the calculated H-bond stretching frequencies of 562 and 541 cm^{-1} (Fig. 3), heterochiral dimer **8b** and homochiral dimer **8a** should be less stable than **9b** and **9a**. This is confirmed by MP2 relative energies of 1.73 and 0.80 kcal/mol (Fig. 3), which is a result of even more intermolecular steric repulsion between the methyl groups. In all these cases, there are additional close intermolecular interactions between CH bonds and the O atom of the other monomer. Each of these interactions involve H,H-repulsion with the positively charged H(O) atom at an even shorter distance. We find that, in the case of **8a**, H,H(O) repulsion is smaller than in **8b**, which lowers the energy of **8a** relative to that of **8b**. In summary, the strength of the (stabilizing) H-bonds in **8** and **9** as reflected by the local H-bond stretching frequencies competes with the (destabilizing) steric interactions between the alkyl groups, and in this way the former provides a simple measure of the steric effects.

Decisive Hydrogen Bonds in Chiral Recognition

Lock-and-key model for chiral recognition in drug design. Often the processes related to the interaction of a chiral drug with a chiral receptor, enzyme or protein, follow a special enantioselective pattern.[12] Pharmaceutical agents are usually synthesized from simple achiral starting materials and, as a result, most chiral drugs are obtained as racemate.[78] There have been several cases in which one enantiomer showed the desired biological activity whereas the other unexpectedly revealed undesirable side effects.[79,80] For example, thalidomide was used in the 1950s and 1960s on pregnant women to avoid morning sickness. The (*R*)-enantiomer is for this purpose the effective form whereas the (*S*)-enantiomer is teratogenic and causes birth defects.[79] Hence, the detailed understanding of chiral recognition and discrimination in drug receptor interactions is of paramount importance.

Xu and coworkers[81] suggested the use of propylene oxide (PO)···glycidol (Gly) complexes (Fig. 4) as simple lock-and-key models simulating drug receptor recognition and binding.[82] PO represents the rigid lock. It is a chiral molecule with a single conformation apart from the internal rotation of the methyl group. Gly is the more flexible key, which can

adjust to the lock in an induced fit manner by rotation at the C-OH and C-CH_2 single bonds. Setting the dihedral angle CCOH to +60°, –60°, and 180° (denoted as + g, –g, and t) and the dihedral angle OCCO to +60°, –60°, and 180° (denoted as + G, –G, and T) nine rotamers result. Gly can bind to the oxygen atom of PO either on the same side (syn) or on the opposite side (anti). Considering that homo- and heterochiral pairs can be formed, this leads to $9 \times 2 \times 2 = 36$ PO···Gly conformations, 18 homochiral and 18 heterochiral forms.

In the following, the four most stable heterochiral (Fig. 4(a) and Table 1) and the four most stable homochiral forms (Fig. 4(b) and Table 1) calculated with ωB97X-D will be discussed. Special emphasis will be laid on the characterization of all H-bonds and their contributions to the complex stability. The most stable complex is the heterochiral form **10a**, which agrees with the MP2 calculations of Xu and coworkers.[81] The next most stable form is the homochiral complex **11a**, with a ΔE value of 0.46 kcal/mol. Complexes **11b**, **10b**, and 1**0c** follow with ΔE values of 0.51, 0.53, and 0.54 kcal/mol. The next group is **10d** and **11c** with $\Delta E = 0.93$ kcal/mol. The least stable complex is **11d** with a ΔE value of 1.28 kcal/mol.

As shown in Figures 4(a) and 4(b), there are three H-bonds in all PO···Gly complexes, with the exception of the least stable complex **11d**. The H-bond (HB1) formed between the oxygen atom of PO and the OH group of Gly is the strongest in all complexes with ω_a values ranging from 617 to 672 cm^{-1}. The second H-bond (HB2) involves one of the hydrogens of the CH_2 part of the PO oxirane and the oxygen of Gly. The third H-bond (HB3) is formed either between the hydrogen atom of the H-CCH_3 group of PO oxirane and the oxygen of Gly or between one of the methyl hydrogen atoms of PO and the oxygen of Gly. As is obvious from the data in Figure 4 and Table 1, HB1 is not decisive for the complex stability. The strongest HB1 bond is found for **10b** with $\omega_a = 672$ cm^{-1} whereas ω_a values of 636 and 634 cm^{-1} are calculated for the most stable complexes **10a** and **11a**. Decisive is HB2, which has not been considered so far.[81] The corresponding ω_a values are 327 cm^{-1} for **10a** and 324 cm^{-1} for **11a**. The corresponding normal mode with highest HB2 contribution possesses a frequency ω_μ at 114 cm^{-1} (59.6% HB2 contribution) for **10a** and at 105 cm^{-1} (64.3% HB2 contribution) for **11a** (see Fig. 4 and Table 1). It is interesting to note that an HB2 bond is not possible in **11d**, the least stable complex, because the CH_2 group of PO points away from the Gly oxygen.

This example shows that it is not necessarily the strongest H-bond that decides the complex stability and chiral differentiation. Additional H-bonds can change relative stabilities. Recently, Scuderi and coworkers reported the same observation in the case of cis-1-amino-2-indanol complexed by methyl-lactate and protonated dimers of *Cinchona* alkaloids.[15] By analyzing the relevant local modes the necessary information is obtained to identify the decisive interaction in case of multiple H-bonds and to quantify them.

CONCLUSIONS

In Table 1, we list the frequencies of these normal modes that possess the highest H-bonding character. In most cases, the relative order of these normal mode frequencies is that of the corresponding local mode frequencies discussed in the previous section. Figure 5 reveals that there is, however, no linear relationship between the local and normal mode frequencies because mode-mode coupling leads to strong changes in the frequencies. In previous work, Cremer and coworkers[44] showed that it is always possible to obtain local mode frequencies from experimental frequencies, no matter whether only some or the complete set of 3*N-L* normal mode frequencies has been measured. Since coupling effects reduce the local H-bond stretching frequencies by 300–400 cm^{-1}, the normal modes, which possess strong H-bond stretching character, can be expected between 100–200 cm^{-1}, i.e., in the FIR.[39]

FIR vibrational spectroscopy and Raman scattering[83,84] have emerged in recent years as a powerful tool in the hands of the chemists and, accordingly, these analytical techniques should be useful in connection with the chiral discrimination of the diastereomers of H-bonded dimers. The analysis presented here suggests that a two-pronged approach, combining FIR measurements with computations, will be successful in this connection. This is outlined in Scheme 1 and implies the measurement of IR-active frequencies in the FIR, their conversion into local mode frequencies with the help of reliable quantum chemical calculations (improved, if needed, by anharmonicity calculations to obtain reliable local mode frequencies[85]), and the identification of H-bond stretching frequencies, which can be used chiral discrimination. The vibrational analysis always requires the reliable calculation of chirodiastaltic energies to verify whether H-boding is the only decisive non-covalent interaction.

In this work, we have focused on calculated local H-bond stretching frequencies to successfully differentiate between homo- and heterochiral diastereomers of H-bonded peroxide, trioxide, hydrazine, glycidol, and butan-2-ol dimers. In addition, we have investigated propylene oxide···glycidol complexes as simple lock-and-key models simulating drug receptor recognition and binding and have rationalized their chirodiastaltic energy differences on the basis of the local mode frequency analysis. Currently, we are extending these investigations to more complicated intermolecular interactions, which involve H-bonding to aromatic ring systems with a focus on dispersion and the decisive role of CH···O interactions. For example, we are investigating how secondary H-bonds controlled by stereochemical factors are decisive for the molecular recognition between (*R*)-(+)-2 napthyl-ethanol and methyl-lactate or between (*R*)-(+)-2 napthyl-ethanol and butanol.

ACKNOWLEDGMENT

This work was financially supported by Grant CHE 1152357 of the National Science Foundation. We thank SMU for providing computational resources.

LITERATURE CITED

1. Lough J, Wainer I. Chirality in natural and applied science. London: Blackwell Science; 2002.
2. Yamamoto H, Carreira, EM, editors. Comprehensive chirality. New York: Elsevier Science; 2012.
3. Amabilino D, editor. Chirality at the nanoscale: nanoparticles, materials, and more. Weinheim: Wiley-VCH; 2009.
4. Nandi N. Chirality in biological systems. Boca Raton, FL: CRC Press; 2011.
5. Guijarro A, Yus M. The origin of chirality in the molecules of life: a revision from awareness to the current theories and perspectives of this unsolved problem. Cambridge: Royal Society of Chemistry; 2008.

6. Meierhenrich U, Kagan, HB. Amino acids and the asymmetry of life: caught in the act of formation. New York: Springer; 2010. (Advances in astrobiology and biogeophysics).
7. Pietropaolo A. Chirality in biochemistry: a computational approach for investigating biomolecule conformations. In: Pignataro B, editor. Ideas in chemistry and molecular sciences: where chemistry meets life. New York: Wiley; 2010. p 291–312.
8. Stalcup AM. Chiral separations. Annu Rev Anal Chem 2010;3:341–363.
9. Ward T, Ward K. Chiral separations: a review of current topics and trends. Anal Chem 2012;84:626–635.
10. Taylor MS, Jacobsen EN. Asymmetric catalysis by chiral hydrogen-bond donors. Angew Chem Int Ed 2006;45:1520–1543.
11. Uraguchi D. Chiral organic ion pair catalysts assembled through a hydrogen-bonding network. Science 2009;120:120–123.
12. Lin G-Q, You Q-D, Cheng J. Chiral drugs: chemistry andbiological action. New York: Wiley; 2011.
13. Brooks W, Guida W, Daniel K. The significance of chirality in drug design and development. Curr Topics Med Chem 2011;11:760–770.
14. Hobza P, Zahradnik R, Muller-Dethlefs K. The world of non-covalent interactions: 2006. Coll Czech Chem Commun 2006;71:443–531.
15. Scuderi D, Le Barbu-Debus K, Zehnacker A. The role of weak hydrogen bonds in chiral recognition. Phys Chem Chem Phys 2011;13:17916–17929.
16. Crego-Calama M, Reihoudt D, editors. Supramolecular chirality. New York: Springer; 2010. (Topics in current chemistry).
17. Vasapollo G, Del Sole R, Mergola L, Lazzoi M, Scardino A, Scorrano S, Mele G. Molecularly imprinted polymers: present and future prospective. Int J Mol Sci 2011;12:5908–5945.
18. Safont-Sempere M, Osswald P, Stolte M, Grüne M, Renz M, Kaupp M, Radacki K, Braunschweig H, Würthner F. Impact of molecular flexibility on binding strength and self-sorting of chiral π-surfaces. J Am Chem Soc 2011;133:9580–9591.
19. Mason S. Molecular optical activity and the chiral discriminations. Cambridge, UK: Cambridge University Press; 2009.
20. Nandi N. Chiral discrimination in the confined environment of biological nanospace: reactions and interactions involving amino acids and peptides. Int Rev Phys Chem 2009;28:111–167.
21. Alkorta I, Picazo O, Elguero J. Theoretical studies on chiral discrimination. Curr Org Chem 2006;10:695–714.
22. Zehnacker A, editor. Chiral recognition in the gas phase. Boca Raton, FL: CRC Press; 2010.
23. Zehnacker A, Suhm MA. Chirality recognition between neutral molecules in the gas phase. Angew Chem Int Ed 2008;47:6970–6992.
24. Portmann S, Inauen A, Luthi HP, Leutwyler S. Chiral discrimination in hydrogen-bonded complexes. J Chem Phys 2000;113:9577–9585.
25. Schäfer R, Schmidt P. Methods in physical chemistry. New York: Wiley; 2012.
26. Mons M, Piuzzi F, Dimicoli I, Zehnacker A, Lahmani F. Binding energy of hydrogen-bonded complexes of the chiral molecule 1-phenylethanol, as studied by 2C-R2PI: comparison between diastereoisomeric complexes with butan-2-ol and the singly hydrated complex. Phys Chem Chem Phys 2000;2:5065–5070.
27. Cremer D, Kraka E. From molecular vibrations to bonding, chemical reactions, and reaction mechanism. Curr Org Chem 2010;14:1524.
28. Freindorf M, Kraka E, Cremer D. A comprehensive analysis of hydrogen bond interactions based on local vibrational modes. Int J Quantum Chem 2012;112:3174–3187.
29. Crawford T, Tam M, Abrams M. The current state of ab initio calculations of optical rotation and circular dichroism spectra. J Phys Chem A 2007;111:12057–12068.
30. Autschbach J. Computing chiroptical properties with first-principles theoretical methods: background and illustrative examples. Chirality 2009;21:E116–E152.
31. Gordillo-Román B, Camacho-Ruiz J, Bucio M, Joseph-Nathan J. Chiral recognition of diastereomeric 6-cedrols by vibrational circular dichroism. Chirality 2012;24:147–154.
32. Del Bene JE, Alkorta I, Elguero J. Do corresponding coupling constants in hydrogen-bonded homo- and hetero-chiral dimers differ? Can J Chem 2010;88:694–699.
33. King AK, Howard BJ. A microwave study of the hetero-chiral dimer of butan-2-ol. Chem Phys Lett 2001;348:343–349.
34. Le Barbu-Debus K, Broquier M, Mahjoub A, Zehnacker-Rentien A. Chiral recognition in jet-cooled complexes of (1R,2S)-(+)-cis-1-amino-2-indanol and methyl lactate: on the importance of the CH$\cdots\pi$ interaction. Phys Chem Chem Phys 2009;11:7589–7598.
35. Le Barbu-Debus K, Guchhait N, Zehnacker-Rentien A. Electronic and infrared spectroscopy of jet-cooled (+/−)-cis-1-amino-indan-2-ol hydrates. Phys Chem Chem Phys 2007;9:4465–4471.
36. Qiu S, Li G, Wang P, Jia G, Feng Z, Li C. Hydrogen bonding in homochiral dimers of hydroxyesters studied by Raman optical activity spectroscopy. J Raman Spectrosc 2011;43:503–513.
37. Zielke P, Suhm M. Raman jet spectroscopy of formic acid dimers: low frequency vibrational dynamics and beyond. Phys Chem Chem Phys 2007;9:4528–4534.
38. Borho N, Häber T, Suhm M. Chiral self-recognition in the gas phase: the case of glycidol dimers. Phys Chem Chem Phys 2001;3:1945.
39. Zou W, Kalescky R, Kraka E, Cremer D. Relating normal vibrational modes to local vibrational modes with the help of an adiabatic connection scheme. J Chem Phys 2012;137:084114.
40. Konkoli Z, Cremer D. A new way of analyzing vibrational spectra. I. Derivation of adiabatic internal modes. Int J Quantum Chem 1998;67:1–9.
41. Konkoli Z, Cremer D. A new way of analyzing vibrational spectra. III. Characterization of normal vibrational modes in terms of internal vibrational modes. Int J Quantum Chem 1998;67:29–40.
42. Xue Z, Suhm MA. Adding more weight to a molecular recognition unit: the low-frequency modes of carboxylic acid dimers. Mol Phys 2010;108:2279–2288.
43. Wilson E, Decius J, Cross P. Molecular vibrations. New York: McGraw-Hill; 1955.
44. Cremer D, Larsson J, Kraka E. New developments in the analysis of vibrational spectra: on the use of adiabatic internal vibrational modes. In: Parkanyi C, editor. Theoretical and computational chemistry. Amsterdam: Elsevier; 1998. p 259–327. (Theoretical organic chemistry; vol 5).
45. Kraka E, Larsson JA, Cremer D. Generalization of the Badger rule based on the uses of adiabatic vibrational modes. In: Grunenberg J, editor. Computational spectroscopy: methods, experiments and applications. Weinheim: Wiley-VCH; 2010. p 105–149.
46. McKean D. Individual CH bond strengths in simple organic compounds: effects of conformation and substitution. Chem Soc Rev 1978;7:399–422.
47. Larsson J, Cremer D. Theoretical verification and extension of the McKean relationship between bond lengths and stretching frequencies. J Mol Struct 1999;485:385–407.
48. Henry B. The local mode model and overtone spectra: a probe of molecular structure and conformation. Accounts Chem Res 1987;20:429–435.
49. Chai J-D, Head-Gordon M. Long-range corrected hybrid density functionals with damped atom-atom dispersion corrections. Phys Chem Chem Phys 2008;10:6615–6620.
50. Chai J-D, Head-Gordon M. Systematic optimization of long-range corrected hybrid density functionals. J Chem Phys 2008;128:084106.
51. Thanthiriwatte KS, Hohenstein EG, Burns LA, Sherrill CD. Assessment of the performance of DFT and DFT-D methods for describing distance dependence of hydrogen-bonded interactions. J Chem Theory Comput 2010;7:88–96.
52. Raghavachari K, Trucks GW, Pople JA, Head-Gordon M. A Fifth-order perturbation comparison of electron correlation theories. Chem Phys Lett 1989;157:479–483.
53. Crawford TD, Schaefer HF. An introduction to coupled cluster theory for computational chemists. Rev Comp Chem 2000;14. DOI:10.1002/9780470125915.ch2
54. Cremer D. Møller-Plesset perturbation theory. In: Schleyer P, Allinger N, Clark T, Gasteiger J, Kollman P, Schaefer H, III, Schreiner P, editors. Encyclopedia of computational chemistry. Vol 3. Chichester (UK): Wiley; 1998. p 1706–1735.
55. Cremer D. Møller-Plesset perturbation theory: from small molecule methods to methods for thousands of atoms. WIREs Comput Mol Sci 2011;1:509–530.
56. Dunning TH, Jr. Gaussian basis sets for use in correlated molecular calculations. I. The atoms boron through neon and hydrogen. J Chem Phys 1989;90:1007–1023.
57. Kendall R, Dunning T, Jr, Harrison R. Electron affinities of the first-row atoms revisited. Systematic basis sets and wave functions. J Chem Phys 1992;96:6796–6806.

58. Kraka E, Grafenstein J, Filatov M, Joo H, Izotov D, Gauss J. COLOGNE12. Southern Methodist University; 2012.
59. Reed A, Weinstock R, Weinhold F. Natural-population analysis. J Chem Phys 1985;83:735–746.
60. Carpenter J, Weinhold F. Analysis of the geometry of the hydroxymethyl radical by the "different hybrids for different spins" natural bond orbital procedure. J Mol Struct (THEOCHEM) 1988;169:41–62.
61. Reed A, Curtiss L, Weinhold F. Intermolecular interactions from a natural bond orbital, donor-acceptor viewpoint. Chem Rev 1988;88:899–926.
62. Frisch M, Trucks GW, Schlegel HB, Scuseria GE, Robb MA, Cheeseman JR, Scalmani G, Barone V, Mennucci B, Petersson GA, Nakatsuji H, Caricato M, Li X, Hratchian HP, Izmaylov AF, Bloino J, Zheng G, Sonnenberg JL, Hada M, Ehara M, Toyota K, Fukuda R, Hasegawa J, Ishida M, Nakajima T, Honda Y, Kitao O, Nakai H, Vreven T, Montgomery JA, Jr, Peralta JE, Ogliaro F, Bearpark M, Heyd JJ, Brothers E, Kudin KN, Staroverov VN, Kobayashi R, Normand J, Raghavachari K, Rendell A, Burant JC, Iyengar SS, Tomasi J, Cossi M, Rega N, Millam JM, Klene M, Knox JE, Cross JB, Bakken V, Adamo C, Jaramillo J, Gomperts R, Stratmann RE, Yazyev O, Austin AJ, Cammi R, Pomelli C, Ochterski JW, Martin RL, Morokuma K, Zakrzewski VG, Voth GA, Salvador P, Dannenberg JJ, Dapprich S, Daniels AD, Farkas Ö, Foresman JB, Ortiz JV, Cioslowski J, Fox DJ. GAUSSIAN09. Wallingford (CT): Gaussian, Inc.; 2009.
63. Cremer D, Pople J. A general definition of ring puckering coordinates. J Am Chem Soc 1975;97:1354–1358.
64. Cremer D, Pople J. Molecular orbital theory of the electronic structure of organic compounds. 23. Pseudorotation in saturated five-membered ring compounds. J Am Chem Soc 1975;97:1358–1367.
65. Cremer D, Szabo K. Ab initio studies of six-membered rings, present status and future developments. In: Juaristi E, editor. Methods in stereochemical analysis, conformational behavior of six-membered rings, analysis, dynamics, and stereoelectronic effects. New York: VCH Publishers; 1995. p 59–135.
66. Cremer D. Theoretical determination of molecular structure and conformation. 1. The role of basis set and correlation effects in calculations on hydrogen peroxide. J Chem Phys 1978;69:4440–4455.
67. Lee J. Accurate structure and torsional barrier heights of hydrogen peroxide. Chem Phys Lett 2002;359:440–445.
68. Koput J. An ab initio study on the equilibrium structure and torsional potential energy function of hydrogen peroxide. Chem Phys Lett 1995;236:516–520.
69. Albright T, Burdett J, Whangbo M. Orbital interactions in Chemistry. New York: Wiley; 1985.
70. Kalescky R, Zhou W, Kraka E, Cremer D. Local vibrational modes of the water dimer— comparison of theory and experiment. Chem Phys Lett 2012;554:243–247.
71. Cremer D. Theoretical determination of molecular structure and conformation. 2. Hydrogen trioxide—a model compound for studying the conformational modes of geminal double rotors and five-membered rings. J Chem Phys 1978;69:4456–4471.
72. Borho N, Suhm M. Glycidol dimer: anatomy of a molecular handshake. Phys Chem Chem Phys 2002;4:2721–2732.
73. Maris A, Giuliano B, Bonazzi D, Caminati W. Molecular recognition of chiral conformers: a Rotational study of the dimers of glycidol. J Am Chem Soc 2008;130:13860–13861.
74. Kahn K, Bruice T. Systematic convergence of energies with respect to basis set and treatment of electron correlation: focal-point conformational analysis of methanol. J Chem Phys 2004;111:18–24.
75. Xu L, Lees R, Hougen J. On the physical interpretation of torsion-rotation parameters in methanol and acetaldehyde: Comparison of global fit and ab initio results. J Chem Phys 1999;110:3835–3842.
76. Christen D, Coudert L, Larsson J, Cremer D. The rotational-torsional spectrum of the g'Gg conformer of ethylene glycol: elucidation of an unusual tunneling path. J Mol Spectrosc 2001;205:185–196.
77. Borho N. Göttingen, Germany: University of Göttingen; 2001.
78. Ali I, Gupta V, Aboul-Enein H, Singh P, Sharma B. Role of racemization in optically active drugs development. Chirality 2007;19:453–463.
79. Eriksson T, Bjorkman S, Hoglund P. Clinical pharmacology of thalidomide. Eur J Clin Pharmacol 2001;57:365–376.
80. Holtman J, Crooks P, Johnson-Hardy J, Wala E. The analgesic and toxic effects of nornicotine enantiomers alone and in interaction with morphine in rodent models of acute and persistent pain. Pharmacol Biochem Behav 2010;94:352–362.
81. Thomas J, Sunahori FX, Borho N, Xu Y. Chirality recognition in the glycidol···propylene oxide complex: a rotational spectroscopic study. Chemistry 2011;17:4582–4587.
82. Borho N, Xu Y. Tailoring the key in a molecular lock-and-key model system: the propylene oxide···2-fluoroethanol complex. J Am Chem Soc 2008;130:5916–5921.
83. Simmen B, Weymuth T, Reiher M. How many chiral centers can Raman optical activity spectroscopy distinguish in a molecule? J Phys Chem A 2012;116:5410–5419.
84. Nafie LA. Vibrational optical activity: principles and applications. New York: Wiley; 2011.
85. Barone V. Anharmonic vibrational properties by a fully automated second-order perturbative approach. J Chem Phys 2005;122:014108–014109.